Optical dielectric function and infrared absorption of hydrogenated amorphous silicon nitride films: Experimental results and effective-medium-approximation analysis

Z. Yin and F. W. Smith
Department of Physics, City College of the City University of New York, New York, New York 10031
(Received 27 December 1989)

The optical dielectric function ϵ (1.5–6.5 eV), ir absorption (400–4000 cm^{-1}), and film density have been measured for a series of hydrogenated amorphous silicon nitride (a-$Si_xN_yH_z$) films deposited at 400 °C via rf plasma-enhanced chemical vapor deposition for varying $[NH_3]/[SiH_4]$ ratios R. From a detailed analysis of the ir and density results, the concentrations of Si—N, N—H, Si—H, and Si—Si bonds and of Si, N, and H atoms have been obtained for the films studied. An effective-medium-approximation analysis of the measured ϵ based on the Si-centered tetrahedron model presented in the preceding paper has provided a more sensitive means of determining the concentration of Si—Si bonds in the films and has demonstrated that careful measurements of ϵ_1 and ϵ_2 can serve as a useful probe of the bonding in these alloys. Approximately 9×10^{20} Si—Si bonds/cm^3 have been found in N-rich films which are close in composition to silicon diimide, $Si(NH)_2$, and these Si—Si bonds have been found to have a significant influence on both the optical energy gap E_{opt} and the refractive index n of the films. New results obtained from the ir absorption measurements include the identification of (1) a shoulder near 1030 cm^{-1} on the main 880-cm^{-1} Si—N(s) band and (2) a weak absorption feature near 640 cm^{-1} which is not hydrogen related. It has been found that the N-rich diimidelike films prepared here have very low porosities and are thermally stable up to 700 °C, properties which will be important for their future applications.

I. INTRODUCTION

Silicon nitride films have been deposited via a variety of chemical-vapor-deposition (CVD) techniques, including plasma-enhanced CVD (PECVD), and have a wide range of applications in microelectronics as passivation layers, diffusion barriers, and insulators.[1] In addition, PECVD silicon nitride films have recently been used as gate dielectrics in applications requiring low deposition temperatures, such as hydrogenated amorphous silicon thin-film transistors.[2] These films are generally referred to as hydrogenated amorphous silicon nitride (a-$Si_xN_yH_z$) and have physical, electrical, and optical properties which are strongly dependent on the film composition, i.e., the [N]/[Si] ratio y/x and the hydrogen content z. Although the incorporation of considerable amounts of hydrogen (up to 30–40 at. %) can have a negative influence on certain film properties such as thermal stability,[3] it has been demonstrated recently[4] that N-rich films ($[N]/[Si]>\frac{4}{3}$) can be deposited with compositions approaching that of silicon diimide, a-$Si(NH)_2$, and that these films can serve as useful low-temperature dielectric layers.[5] In addition, such polymeric layers can be relatively stable thermally, apparently up to at least 600 °C.[6]

It is clearly important to establish as close a correlation as possible between the macroscopic properties of these a-$Si_xN_yH_z$ films and the film microstructure, i.e., the local atomic bonding configurations involving the Si, N, and H atoms. We report here on detailed measurements of infrared absorption, film density ρ, and optical dielectric function ϵ for several a-$Si_xN_yH_z$ films, focusing on films which are N-rich. The bond and atom concentrations obtained from the ir absorption and film density measurements are compared with those obtained from an effective-medium-approximation (EMA) analysis of the measured ϵ of the film. This EMA analysis is based on the microstructural model presented in paper I (Ref. 7) in which Si-centered tetrahedra are considered to be the fundamental structural units which determine the optical response of the films. This analysis has yielded results for the bond and atom concentrations which are consistent with those obtained from the ir absorption and film density measurements for the N-rich films, thus confirming the applicability of the microstructural model to the alloys studied.

It has also been possible to specifically address the issue of the existence of Si—Si bonds in the films studied. This is an important point since it has been suggested recently[8] that these bonds are potentially harmful defects in the a-$Si_xN_yH_z$ films used in device applications. The dependence of the concentration of Si—Si bonds on the deposition conditions and their effect on film properties will be discussed.

Details of the experimental procedure will be presented in Sec. II, followed by the results and analysis of the various measurements in Sec. III. The EMA analysis for ϵ will appear in Sec. IV, with discussion and conclusions following in Sec. V.

II. EXPERIMENT

The a-$Si_xN_yH_z$ films studied here were prepared via rf (13.56 MHz) plasma-enhanced CVD in a stainless-steel deposition system which has been described previously.[9]

©1990 The American Physical Society

Undiluted silane and ammonia were delivered via separate lines to the deposition chamber, with typical deposition parameters as follows (see Table I): substrate temperature $T_s = 400\,°C$, discharge power of 0.43 W/cm^2, total pressures of 0.5 or 0.15 Torr, flow rates of 100 or 60 sccm (cubic centimeters per minute at STP) for NH_3 and variable flow rates for SiH_4 to obtain the desired ratios $R = [NH_3]/[SiH_4] = 10$, 20, or 40. The substrates, polished clear fused quartz for measurements of ϵ, intrinsic Si (polished both sides) for measurements of ir absorption and film composition, and Al foils for density measurements, were mounted on the powered electrode.

For the determination of the optical dielectric function $\epsilon = \epsilon_1 + i\epsilon_2$ of these a-$Si_xN_yH_z$ films, measurements of film transmittance and of the reflectance from the free surface of the film have been carried out from 1.5–6.5 eV using an Aviv 14DS uv-visible spectrophotometer. For these reflectance measurements, the calibration of an NBS standard mirror has been extended from 4.9 up to 6.7 eV using the known optical constants[10] of a polished Si wafer. Details of the analysis procedure for obtaining n and k, the real and imaginary parts of the index of refraction, and film thickness d have been given previously.[9] Values of the optical energy gap E_{opt} have been obtained from plots of $E\epsilon_2^{1/2}$ versus energy E, using the Tauc relation.[11]

Infrared measurements were carried out using a Digilab FTS-40 Fourier transform infrared spectrophotometer in the range from 400 to 4000 cm^{-1}, with a resolution of 8 cm^{-1}. Absorbances for the various absorption modes [N—H(stretching), Si—N(stretching), etc.] have been obtained from the measured film absorbance by subtracting a fitted baseline to account for interference effects in the film itself. The ir absorption of the $R = 40, P = 0.15$ Torr film has also been measured as a function of the annealing of the film up to 1000 °C. Film densities have been obtained from the masses of the films, determined by weighing the Al-foil substrates before and after deposition, and the film volumes, obtained from measurements of film area and the average thickness. Information concerning film composition has been obtained via depth profiling using a Perkin-Elmer PHI 600 scanning Auger microprobe. The depth profile of each film was obtained by sputtering using a 3-keV Ar^+-ion beam.

III. RESULTS AND ANALYSIS

a-$Si_xN_yH_z$ films have been prepared using $[NH_3]/[SiH_4]$ ratios R of 10, 20, and 40 at $P = 0.5$ Torr and $R = 40$ at 0.15 Torr. The deposition rates for these films are given in Table I where it can be seen that R_{dep} decreases from 320 to 200 Å/min as R increases from 10 to 40 at $P = 0.5$ Torr. R_{dep} then decreases further to 60 Å/min at $R = 40$ and $P = 0.15$ Torr. It is clear that the deposition rates are limited primarily by the availability of Si, i.e., by the flow rates of SiH_4 into the deposition chamber (see Table I). This result is reasonable, given the large excess of NH_3 relative to SiH_4 present during the depositions. Film compositions (x, y, and z) have been determined in two ways, the first using ir absorption and film density measurements and the second in addition using measurements of ϵ to obtain the concentration of Si—Si bonds. These analyses are presented below, in Secs. III B and IV, respectively.

The infrared absorption and film density results will now be presented, followed by the analysis for the bond and atom concentrations and the results for ϵ. The EMA analysis for ϵ based on the Si-centered tetrahedron model is presented in Sec. IV.

A. ir absorption and film density

The ir absorption spectra for the $R = 10$ and $R = 40$ films prepared at $T_s = 400\,°C$ and $P = 0.5$ Torr are shown in Fig. 1 in the range from 400 to 4000 cm^{-1}. Note that interference effects in the films have already been removed from these spectra via the baseline correction procedure. Absorption bands for the N—H(stretching) mode have been observed near 3320 cm^{-1}, for Si—H(stretching) near 2180 cm^{-1}, for H—N—H(bending) near 1550 cm^{-1}, for N—H(bending) near 1180 cm^{-1}, for Si—N(stretching) near 880 cm^{-1}, and for Si—N(breathing) near 480 cm^{-1}. The weak features seen near 2320 cm^{-1} result from an incomplete subtraction of the absorption due to CO_2 in the spectrophotometer sample chamber. The film thicknesses d, peak wave numbers ν(peak), maximum absorption coefficients α(max), full widths at half maximum (FWHM), and normalized absorption band areas $\int \alpha d\nu$ for these bands are listed in Table II for the four alloy

TABLE I. Deposition parameters and properties of a-$Si_xN_yH_z$ films studied.

Sample	T_s (°C)	P (Torr)	R $[NH_3]/[SiH_4]$	R_{dep} (Å/min)	ρ[a] (g/cm^3)	n[b]	E_{opt}[c] (eV)
1	400	0.5	100/10=10	320	2.49	1.86	3.83
2	400	0.5	100/5=20	280	2.24	1.84	5.05
3	400	0.5	100/2.5=40	200	2.08	1.79	5.20
4	400	0.15	60/1.5=40	60	2.18	1.82	5.42

[a]Film density; typical uncertainty is ±0.1 g/cm^3.
[b]Index of refraction at 1.5 eV; typical uncertainty is ±0.02.
[c]Optical energy gap; typical uncertainty is ±0.1 eV.

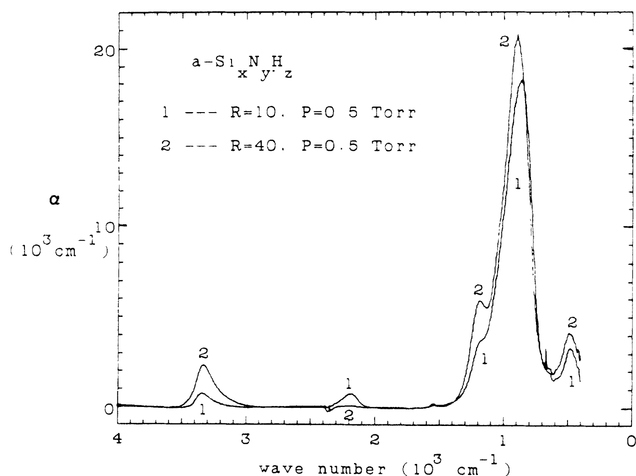

FIG. 1. Absorption coefficient α vs wave number for the $R=[NH_3]/[SiH_4]=10$ and 40 a-$Si_xN_yH_z$ films prepared at $T_s=400\,^{\circ}C$ and $P=0.5$ Torr.

films studied, along with the results for absorption bands which have been identified as being present near 1030 and 640 cm^{-1} from deconvolutions of the main absorption band, an example of which is shown in Fig. 2 for the $R=40, P=0.5$ Torr film.

It is important to note here that, for a given alloy, measurable changes in the peak position and FWHM of the main Si—N(stretching) band have been observed for films of different thicknesses prepared under identical conditions. For example, the Si—N(stretching) peak positions are about 20 cm^{-1} higher for thicker films ($d=0.5-1.0$ μm) than for thinner films ($d=0.1-0.2$ μm). While the FWHM's of the thicker films are also greater by 20–40 cm^{-1} than the FWHM's for the thinner films, the normalized Si—N(stretching) absorption band areas have been found to be independent of film thickness, to within experimental error ($\pm5\%$), for the films studied. Thus, the areas of the Si—N(stretching) bands can be used, in principle, to determine bond concentrations for these films (see Sec. III B below). It is clear, however, that correlations of parameters such as index of refraction n within the peak wave number of the Si—N(stretching) band are valid only when carried out for films of comparable thickness. The observed shifts in ν(peak) and α(max) with film thicknesses are due to changes in film reflectance[12] resulting from the strong absorption of the Si—N(stretching) mode.

The N—H(stretching) band near 3320 cm^{-1} is observed to be an asymmetric peak, with a tail extending on the low wave-number side down to about 2900 cm^{-1} (see Fig. 3). This asymmetry is likely to be due at least in part to hydrogen bonding[13] between the H atoms in the N—H bonds and lone-pair electrons on nearby N atoms, which is indicated by the notation N—H · · · N. Also, in the $R=40$ films with higher concentrations of hydrogen, evidence can be seen for increasing absorption due to the stretching modes of the N-H_2 unit between 3400 and 3500 cm^{-1}. In the same films, the H—N—H(bending)

TABLE II. Infrared-absorption results for a-$Si_xN_yH_z$ films.

		Si—N				N—H and Si—H (in parentheses)			
Sample	d (Å)	ν(peak)[a] (cm^{-1})	α(max)[b] (cm^{-1})	FWHM[c] (cm^{-1})	$\int \alpha d\nu$[d] (10^5 cm^{-2})	ν(peak)[a] (cm^{-1})	α(max)[b] (cm^{-1})	FWHM[c] (cm^{-1})	$\int \alpha d\nu$[d] (cm^{-2})
1	9800	877	18 300	223	43.50	3340	810	141	1.36×10^5
($R=10, P=0.5$)		1035	2860	103	3.13	1163	3520	206	7.72×10^5
		478	3150	175	5.85	1543	60	32	1.80×10^3
		631	838	63	0.55	(2184	750	139	11.03×10^4)
2	5930	877	20 200	197	42.35	3317	1860	177	3.89×10^5
($R=20, P=0.5$)		1034	3850	120	4.91	1178	4120	184	8.06×10^5
		487	3700	140	5.53	1547	160	38	6.49×10^3
		644	1230	76	0.99	(2182	310	153	4.93×10^4)
3	12 250	888	20 400	196	42.42	3336	2290	163	4.47×10^5
($R=40, P=0.5$)		1034	4750	130	6.56	1185	5540	178	10.48×10^5
		476	4060	183	7.92	1546	190	42	8.24×10^3
		656	1640	104	1.80				
4	2435	868	20 700	169	37.19	3325	2310	189	5.18×10^5
($R=40, P=0.15$)		1022	4310	125	5.73	1181	3620	158	6.10×10^5
		475	3790	178	7.16	1551	180	46	8.80×10^3
		661	1400	96	1.43				

[a]Peak wave number; typical uncertainty is ±5 cm^{-1}.
[b]Maximum absorption coefficient; typical uncertainty is $\pm4\%$.
[c]Full width at half maximum; typical uncertainty is ±5 cm^{-1}.
[d]Normalized absorption band area $\int \alpha d\nu$, where $\alpha=(2.303/d)A$ is the absorption coefficient; d is the film thickness and A the absorbance. Typical uncertainty is $\pm5\%$.

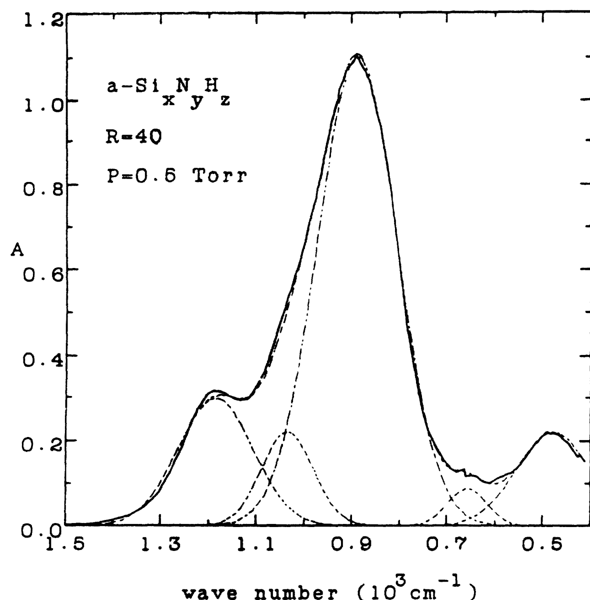

FIG. 2. Absorbance A vs wave number for the $R=40, P=0.5$ Torr film in the range from 1500 to 400 cm^{-1}. The solid curve is the experimental result, while the dashed curves are the individual fitted absorption bands and their sum (see text for discussion).

absorption band near 1550 cm^{-1} is also observed to be stronger. These results are consistent with those of previous studies.[4] Following the anneal of the $R=40, P=0.15$ Torr film at 700 °C, the absorption band at 1550 cm^{-1} was observed to increase, thus providing evidence for the conversion of N—H bonding units to N-H_2 units. This conversion is apparently one of the steps leading to the formation and subsequent evolution of NH_3 molecules from the annealed film.

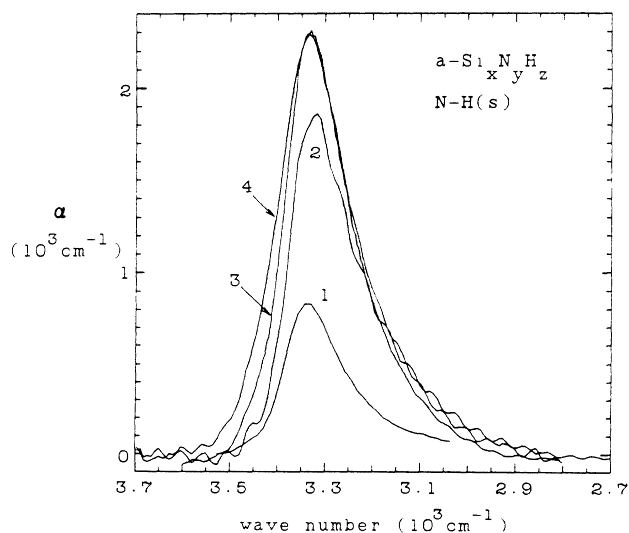

FIG. 3. Absorption coefficient α vs wave number in the N—H(stretching) region from 3700 to 2700 cm^{-1} for the four films studied. See Table I for the numbering of the curves.

Evidence for Si—H(stretching) absorption near 2180 cm^{-1} has been observed only in the films prepared with $R=10$ and $R=20$ (samples 1 and 2, respectively, in Table II). This absorption band appears to consist of two subbands near 2170 and 2250 cm^{-1}, which is consistent with Si—H(stretching) absorption arising from Si-HN$_2$Si and Si-HN$_3$ tetrahedra, respectively.[14]

In order to accurately determine the absorbances of the N—H(bending) band near 1180 cm^{-1} and the Si—N(stretching) band near 880 cm^{-1}, it has been necessary to carry out deconvolutions of the broad region of absorption extending from 400 to near 1500 cm^{-1}. For this purpose, five Gaussian absorption bands have been employed, centered near 1180, 1030, 880, 640, and 480 cm^{-1}. The deconvolution for the $R=40, P=0.5$ Torr film is shown in Fig. 2, and the results of this procedure for all the films studied are presented in Table II. There is only one absorption feature in this region which is clearly hydrogen related, namely, the N—H(bending) band near 1180 cm^{-1}. The absorption band centered near 1030 cm^{-1} is proposed to be a shoulder on the main Si—N(stretching) band near 880 cm^{-1}. The small absorption feature consistently observed in these films near 640 cm^{-1} would normally be assumed to be due to Si—H(rocking, wagging) modes.[15] This cannot be the complete explanation here since this feature has been observed in the $R=40$ films for which there is no evidence for absorption due to the Si—H(stretching) mode near 2180 cm^{-1}. In addition, annealing experiments on these films have shown that, as the hydrogen is driven out of the $R=40$ film via heating up to 1000 °C, no significant changes are observed to occur in the 640 cm^{-1} absorption. We propose instead that this absorption band is due to a vibration of the N—Si$_3$ bonding unit,[16] so that the existence of three absorption bands (near 880, 640, and 480 cm^{-1}) for this unit may be analogous to the observation of three absorption bands (near 1070, 800, and 450 cm^{-1}) for the Si—O—Si bonding unit in a-SiO$_2$ films.[17]

Film density ρ results are shown in Table I for the four alloys studied and it can be seen that ρ is a decreasing function of R, the [NH$_3$]/[SiH$_4$] ratio. As will be seen later, increasing R results in a decrease of the Si atomic fraction x and an increase in the H atomic fraction z in these a-Si$_x$N$_y$H$_z$ films, so that, as expected, ρ decreases with increasing H content of the films.[18] There is a small increase observed in ρ for the $R=40, P=0.15$ Torr film, which may be related to the lower deposition rate measured for this film.[19]

B. Bond and atom concentrations

The concentrations of N—H, Si—H, and Si—N bonds in these alloys have been obtained from the normalized ir absorption band areas presented in Table II, using the expression

$$N(X-Y)=K(X-Y)\int \alpha(\nu)d\nu , \tag{1}$$

where $N(X-Y)$ is the concentration of $X-Y$ bonds, $K(X-Y)$ is their ir absorption cross section, and the normalized area is given by the wave-number integral of

the absorption coefficient α over the band in question. The bands used for this purpose are the 3320-cm^{-1} N—H(stretching) band, the 2180-cm^{-1} Si—H(stretching) band, and the sum of the Si—N(stretching) bands near 880 and 1030 cm^{-1}. Values of K(N—H)$=8.2\times10^{16}$ cm^{-1} and K(Si—H)$=5.9\times10^{16}$ cm^{-1} have been obtained from the results of Lanford and Rand[20] [using $K=1/(2.303\sigma)$], while the results K(Si—N)$=1.82\times10^{16}$ and 2.1×10^{16} cm^{-1} have been obtained, respectively, from measurements carried out here for the $R=40, P=0.5$ Torr and $R=40, P=0.15$ Torr films. To obtain these results for K(Si—N), it has been assumed that these two $R=40$ films contain no N—N bonds and that N(Si—Si) $\ll N$(Si—N). These are reasonable working assumptions as these films are N-rich ($y/x\sim1.9$, see Table III) and contain from 36 to 39 at. % H. The densities of Si—N bonds in these two films were obtained in a self-consistent manner using the measured values for N(N—H) and N(Si—H) and the film density ρ, along with the relationships between bond and atom concentrations and ρ presented below [Eqs. (2)–(5)]. Once N(Si—N) was obtained, Eq. (1) was inverted to obtain the results for K(Si—N) quoted above from the measured normalized Si—N(stretching) band areas. Previous estimates[21] of K(Si—N) for films with lower [N]/[Si] ratios have yielded values in the range $(0.9-1.0)\times10^{16}$ cm^{-1}, lower by about a factor of 2 compared to the results obtained here. A more recent analysis[22] carried out for nearly stoichiometric films has obtained the result K(Si—N)$=2.4\times10^{16}$ cm^{-1}, in better agreement with the values obtained here. It is not unreasonable to expect that K(Si—N) will depend on the [N]/[Si] ratio y/x and H content z of the films studied. An alternative approach to obtaining N(Si—N) and, hence, K(Si—N) using the values of N(Si—Si) obtained from the EMA analysis for ϵ will be presented in Sec. IV.

The results obtained here for the concentrations of N—H, Si—H, and Si—N bonds are presented in Table III. For the computation of the experimental uncertainties in the bond concentrations, the accuracies of the cross sections have been assumed to be $\pm5\%$ for K(N—H) and K(Si—H) and $\pm10\%$ for K(Si—N) for the two $R=40$ films. It should be pointed out that the reproducibility of the bond concentrations measured for films of different thicknesses prepared under the same conditions is much better than the estimated absolute accuracies quoted in Table I. It can be seen that N(N—H) and N(Si—N) are increasing functions of R and that both also increase slightly as P decreases from 0.5 to 0.15 Torr. In contrast, N(Si—H) is highest for $R=10$ (6.5×10^{21} cm^{-3}) and then decreases with R, falling to zero to within experimental error (less than about 2×10^{19} cm^{-3}) for the $R=40$ films.

In order to obtain the atom concentrations N(Si), N(N), and N(H) [along with the Si—Si bond concentration N(Si—Si)], the following expressions have been employed:

$$N(\mathrm{Si})=[N(\mathrm{Si—N})+N(\mathrm{Si—H})]/4+N(\mathrm{Si—Si})/2\ , \quad (2)$$

$$N(\mathrm{N})=[N(\mathrm{N—H})+N(\mathrm{Si—N})]/3\ , \quad (3)$$

$$N(\mathrm{H})=N(\mathrm{N—H})+N(\mathrm{Si—H})\ , \quad (4)$$

and

$$\rho=m_{\mathrm{Si}}N(\mathrm{Si})+m_{\mathrm{N}}N(\mathrm{N})+m_{\mathrm{H}}N(\mathrm{H})\ , \quad (5)$$

where the m_i are atomic masses. Note that it has been assumed here that there are no N—N or H—H bonds in the films. From the results for N(N—H), N(Si—H), N(Si—N), and ρ presented in Tables I and III, Eqs. (2)–(5) have been solved for the four unknowns, N(Si), N(N), N(H), and N(Si—Si), with the results also given in Table III. Values for the composition parameters x,y,z, and the [N]/[Si] ratios y/x for these a-$Si_xN_yH_z$ alloys are also given in Table III. Again, the reproducibility of the results obtained for the atom concentrations (and for x, y, and z) is much better than the estimated absolute uncertainties given in Table III. The estimated uncertainties in N(Si—Si) are large, $\pm0.9\times10^{22}$ cm^{-3}, primarily due to the indirect manner in which it has been determined. More reliable results for N(Si—Si) obtained from the EMA analysis for ϵ are given below (see Table IV).

It can be seen from the results presented in Table III that N(Si) is a decreasing function of $R=[NH_3]/[SiH_4]$, as expected, while both N(N) and N(H) increase with increasing R. From the [N]/[Si] ratio, it can be seen that the $R=20$ and the two $R=40$ films are N rich ($y/x>\frac{4}{3}$), with y/x in the range from 1.44 to 1.95. This last value is quite close to the [N]/[Si] ratio of silicon di-

TABLE III. Bond and atom concentrations for a-$Si_xN_yH_z$ films obtained from ir and density measurements.

Sample	Film composition[a] (a-$Si_xN_yH_z$)	y/x[b] [N]/[Si]	N(Si—N)[c] (10^{22} cm^{-3})	N(N—H)[c] (10^{22} cm^{-3})	N(Si—H)[c] (10^{22} cm^{-3})	N(Si—Si)[c] (10^{22} cm^{-3})	N(Si)[d] (10^{22} cm^{-3})	N(N)[d] (10^{22} cm^{-3})	N(H)[d] (10^{22} cm^{-3})
1	$Si_{0.42}N_{0.37}H_{0.21}$	0.88	8.49	1.12	0.65	2.76	3.66	3.20	1.77
2	$Si_{0.27}N_{0.39}H_{0.34}$	1.44	8.60	3.19	0.29	0.96	2.70	3.93	3.49
3	$Si_{0.22}N_{0.42}H_{0.36}$	1.91	8.90	3.66	less than 0.002	less than 0.7	2.23	4.19	3.66
4	$Si_{0.21}N_{0.41}H_{0.38}$	1.95	9.13	4.24	less than 0.008	less than 0.9	2.28	4.46	4.24

[a]Typical uncertainties are ±0.05 for x, ±0.04 for y, and ±0.03 for z.

[b][N]/[Si] ratio; typical uncertainty is $\pm15\%$.

[c]Bond concentrations; typical uncertainties are $\pm8\%$ for N(N—H) and N(Si—H), $\pm10\%$ for N(Si—N), and $\pm0.9\times10^{22}$ cm^{-3} for N(Si—Si).

[d]Atom concentrations; typical uncertainties are $\pm8\%$ for N(N) and N(H) and $\pm0.5\times10^{22}$ cm^{-3} for N(Si).

TABLE IV. Results of EMA analysis for N(Si—Si) and derived values of composition (x,y,z), N(Si—N), and K(Si—N).

Sample	x	y	z	y/x	N(Si—Si) (10^{22} cm^{-3})	N(Si—N) (10^{22} cm^{-3})	K(Si—N) (10^{16} cm^{-1})
1 ($R=10, P=0.5$)	0.35	0.46	0.19	1.31	0.36	11.35	2.43
2 ($R=20, P=0.5$)	0.25	0.41	0.34	1.64	0.15	9.56	2.02
3 ($R=40, P=0.5$)	0.22	0.41	0.37	1.86	0.084	8.79	1.80
4 ($R=40, P=0.15$)	0.21	0.40	0.39	1.91	0.092	9.02	2.10

imide, $Si(NH)_2$. The results for N(Si—Si) are of interest as Si—Si bonds have been proposed to be potentially important defects in these films.[8] It can be seen that this analysis of the ir absorption and film density measurements suggests that there is a significant concentration of Si—Si bonds, 2.76×10^{22} cm^{-3}, in the $R=10$ film, which is equal to about $\frac{1}{3}$ of N(Si—N)$=8.49\times10^{22}$ cm^{-3} for the same film. N(Si—Si) falls to 0.96×10^{22} cm^{-3} for $R=20$ and then to less than $(0.7-0.9)\times10^{22}$ cm^{-3} for the $R=40$ films, values which are equivalent to zero to within the limits of the accuracy of these measurements and the analysis employed. It should be noted that the results obtained here indicate that the presence of Si—Si bonds in these films seems to be correlated with the presence of Si—H bonds (see Table III).

The scanning Auger microprobe (SAM) study has also shown that the [N]/[Si] ratio is an increasing function of R, a result which is consistent with the analysis presented here. A more detailed analysis of the SAM measurements has not been undertaken due to a lack of absolute sensitivity factors for N and Si in the films studied. It should be noted that no evidence for oxygen has been found in the as-deposited films from either the ir absorption studies or from the SAM results. In addition, no evidence has been found for the diffusion of either O_2 or H_2O into the films during the period of 17 months following their initial exposure to the atmosphere. This observation indicates that these films can be prepared with very low porosities.

C. Optical dielectric function ϵ

The measured real part ϵ_1 and imaginary part ϵ_2 of the optical dielectric function ϵ for the four films studied are shown in Fig. 4 as functions of photon energy E between 1.5 and about 6.5 eV. Also shown in Fig. 4 for comparison are the results of Philipp[23] for a CVD a-Si_3N_4 film which was essentially hydrogen free. The indices of refraction n at 1.5 eV and the optical energy gaps E_{opt} for the four films studied are given in Table I. It can be seen from $\epsilon_2(E)$ and E_{opt} that the optical-absorption edge shifts to higher energies with increasing R as stronger Si—N bonds replace weaker Si—Si bonds in the films (see Table III for the bond concentrations). This behavior has been observed previously.[24] The two N-rich films prepared here using $R=40$, and labeled 3 and 4 in Fig. 4, have absorption edges which are higher in energy than that of the CVD film studied by Philipp.[23] Note that ϵ_1 and ϵ_2 are observed to be essentially independent of pressure P for the two $R=40$ films. Also, n decreases with increasing R as the H content of the films increases and the film density falls. All four of the films studied here have values of n which are lower than that of the CVD film studied by Philipp, due to their lower densities resulting from the incorporation of hydrogen.

It has been observed here that thinner a-$Si_xN_yH_z$ films

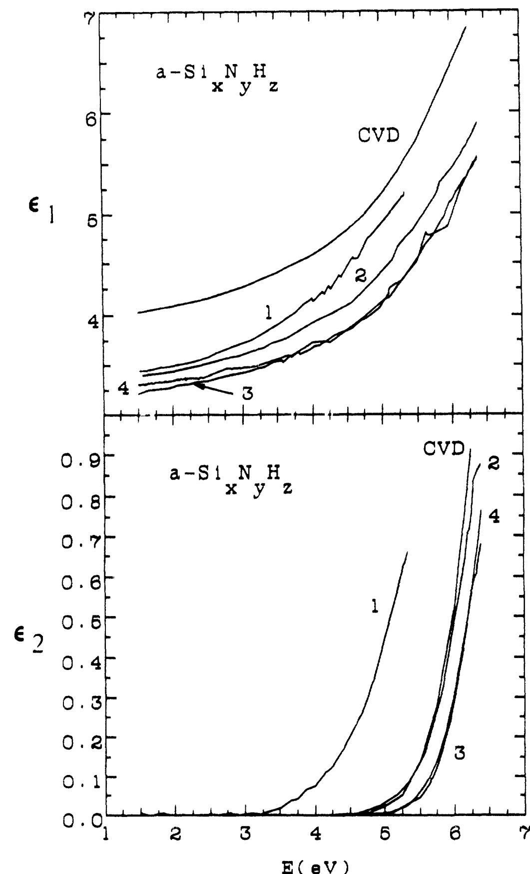

FIG. 4. Real part ϵ_1 and imaginary part ϵ_2 of the optical dielectric function vs energy E, as measured for the four films studied. Also shown are the experimental results of Philipp (Ref. 23) for a CVD a-Si_3N_4 film, labeled CVD. See Table I for the numbering of the other curves.

have higher values of n than thicker films prepared under the same conditions. We believe that this is due to the existence of enhanced concentrations of Si-centered tetrahedra containing Si—Si bonds near the film-substrate interfaces. Such tetrahedra would lead to higher n values and it is clear that this effect would be more important for thin films.

IV. EMA ANALYSIS OF THE OPTICAL DIELECTRIC FUNCTION

The measured optical dielectric function ϵ will now be used within the framework of the Bruggemann effective-medium approximation[25] (EMA) in order to obtain important additional information concerning the microstructure of the films studied. The microstructural model to be employed in the EMA analysis is based on Si-centered tetrahedra. This model has been presented in detail for these a-$Si_xN_yH_z$ alloys in paper I (Ref. 7) and has also been used previously in the analysis of the optical response of hydrogenated amorphous films based on carbon[26] (a-C:H), silicon[27] (a-Si:H), and silicon-based alloys[9,28] (a-Si_xC_{1-x}, a-Si_xO_{1-x}, and a-Si_xN_{1-x}).

The Bruggemann EMA is defined by the following two expressions:

$$\sum_i v_i \frac{\epsilon_i-\epsilon}{\epsilon_i+2\epsilon}=0 \tag{6}$$

and

$$\sum_i v_i=1 \ , \tag{7}$$

where ϵ_i and v_i are the complex optical dielectric function and volume fraction, respectively, of the ith component and ϵ is the measured value for the film. We will also make use of the following relationship for the measured film density ρ:

$$\sum_i v_i\rho_i=\rho \ , \tag{8}$$

where ρ_i is the density of the ith component. The components to be used in the EMA analysis are the Si-centered tetrahedra and the ϵ_i and ρ_i determined for specific tetrahedra in the preceding paper (see Figs. 2–4 and Tables I–III of Ref. 7) will be used in Eqs. (6)–(8) along with the measured ϵ and ρ in order to determine the tetrahedron volume fractions v_i appropriate for the films under consideration. The goal of this EMA analysis is to obtain independent estimates for the bond and atom concentrations which can be compared with the results previously obtained from the analysis of ir absorption and film density measurements presented in Sec. III. It will be particularly interesting to attempt to confirm the results already obtained for N(Si—Si). It should be pointed out that an advantage of the EMA analysis is that information can be obtained concerning not only the concentrations of bonds and atoms, but also the manner in which the bonds and atoms are incorporated into the Si-centered tetrahedra.

Table IV presents the results of the EMA analysis for the N(Si—Si) bond concentrations of the four films studied. The analysis for each film has employed only those tetrahedra which are necessary to model the optical response and which are consistent with the film composition and density. The analysis and results for each alloy film will now be briefly discussed, beginning with the two N-rich films.

A. Sample 3 ($R=40, P=0.5$ Torr)

For this N-rich a-$Si_xN_yH_z$ film, the five Si-centered tetrahedra, Si-$N_{4-i}(NH)_i$, $i=0$–4, provide the dominant contribution to the measured ϵ and ρ. With these five tetrahedra, however, it has not been possible to obtain a satisfactory fit to the measured ϵ_2 and so an additional tetrahedron containing a Si—Si bond has been included in the EMA analysis. The addition of the Si-Si$(NH)_3$ tetrahedron leads to a shift of the onset of ϵ_2, i.e., the absorption edge, to lower energies, in better agreement with experiment. The comparison between the measured and fitted ϵ for this alloy film is shown in Fig. 5(a) where it can be seen that satisfactory agreement has been obtained. The concentration N(Si—Si) of Si—Si bonds resulting from this analysis is 8.3×10^{20} cm^{-3}, which is in fact consistent with the upper limit of 7×10^{21} cm^{-3} previously obtained from the analysis of the ir absorption and film density measurements (Table III). The results of the EMA fit for the film composition, density, and N—H and Si—N bond concentrations for this film all agree with the results of the ir absorption and the film density analysis presented in Table III, to within experimental error.

B. Sample 4 ($R=40, P=0.15$ Torr)

The EMA analysis for this N-rich film has employed the same six Si-centered tetrahedra which were used for sample 3, see above, and the resulting fit to the measured ϵ has also been quite satisfactory. The value of N(Si—Si) obtained, 9.2×10^{20} cm^{-3}, is again consistent with the upper limit of 9×10^{21} cm^{-3} previously obtained.

C. Samples 1 ($R=10, P=0.5$ Torr) and 2 ($R=20, P=0.5$ Torr)

Evidence for the presence of Si—H bonds has been found in the ir absorption spectra of these two films and so additional tetrahedra containing Si—H bonds have been used in the EMA analysis. For the $R=10$ film the following five tetrahedra have been employed: Si-$N_2(NH)_2$, Si-HN_2(NH), Si-HN$(NH)_2$, Si-SiN_2(NH), and Si-Si_2N_2. Although a reasonable fit to the measured ϵ can be obtained, the fitting procedure is not unique. One result which has been confirmed, however, is that a Si-centered tetrahedron containing two Si—Si bonds is required to obtain even a qualitative fit to the measured ϵ_2 for this alloy. The EMA analysis has yielded N(Si—Si)$=3.6\times10^{21}$ cm^{-3} for this $R=10$ film. A void component with a volume fraction of 0.06 has been used to obtain the fit for this alloy.

For the $R=20$ film, the five Si-$N_i(NH)_{4-i}$, $i=0$–4, tetrahedra along with two tetrahedra containing Si—Si

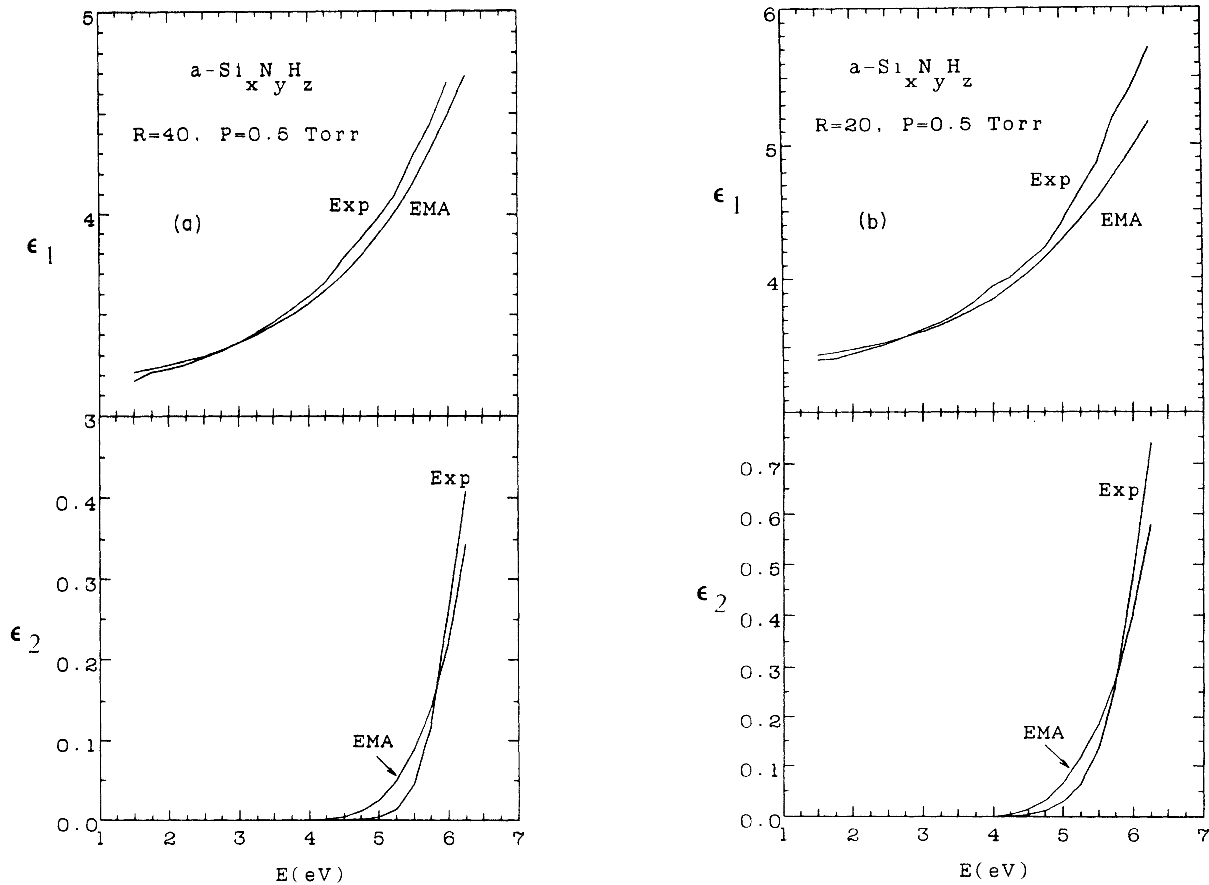

FIG. 5. Comparison between the measured and fitted optical dielectric functions $\epsilon=\epsilon_1+i\epsilon_2$ for the (a) $R=40$ and (b) $R=20$, $P=0.5$ Torr films. Exp, measured ϵ; EMA, fitted result of EMA analysis (see text).

bonds and two containing Si—H bonds have been employed in the EMA analysis. The results of this fit are shown in Fig. 5(b) and it can be seen that reasonable agreement has been obtained with experiment. For this alloy tetrahedra containing just one Si—Si bond are sufficient to obtain the fit shown and the EMA analysis has yielded $N(\text{Si—Si})=1.5\times10^{21}\ \text{cm}^{-3}$.

The results for N(Si—Si) for these last two alloy films obtained from this EMA analysis are systematically lower than those obtained from the analysis of the ir absorption and film density results by about a factor of 7 (see Table III). These lower values of N(Si—Si) are more reliable as the EMA analysis emphasizes the film absorption which is directly related to the presence of Si—Si bonds in the films. The analysis involving the ir absorption and film density measurements is, in principle, also capable of yielding reliable results, but unfortunately this analysis involves the use of ir absorption cross sections, particularly K(Si—N), whose determination is difficult to achieve with high accuracy.

The values of N(Si—Si) obtained here from the EMA analysis have been used in Eqs. (2)–(5), along with the measured values of N(Si—H) and N(N—H) (Table III) and of film density ρ (Table I), in order to determine more reliable values for N(Si—N) and the compositions (x,y,z) of the alloys studied. The results of this analysis are also presented in Table IV. The results obtained for the two $R=40$ films are in good agreement with these obtained via the previous analysis (see Table III). For the $R=10$ and 20 films, on the other hand, this analysis has yielded higher values for y and lower values for x than obtained previously. The resulting higher [N]/[Si] ratios y/x are in fact more consistent with the results of the SAM measurements.

Also given in Table IV are values for the ir absorption cross section K(Si—N) determined from the values of N(Si—N) given in Table IV and the measured normalized ir absorption band areas for Si—N(stretching) presented in Table II. These values are consistent with those derived in Sec. III B for the two $R=40$ films, while the value for $R=10$ is in good agreement with the results of a recent analysis[22] for nearly stoichiometric films.

V. DISCUSSION AND CONCLUSIONS

The microstructural model which appears to be appropriate for these $a\text{-Si}_x\text{N}_y\text{H}_z$ alloy films and which is consistent with the results obtained here is the one presented in paper I.[7] This model is essentially the random-bonding model (RBM) originally proposed by Philipp[23,29] in which Si-centered tetrahedra are the fundamental structural units which determine the optical

response of the films. The RBM, however, needs to be generalized for these alloys as the bonding is not actually completely random. Instead, there is strong evidence for chemical ordering in the sense that there is a preferential tendency for the formation of Si—N and N—H bonds in the N-rich alloys. This should not be surprising since in the two important stable compounds in the Si:N:H alloy system, i.e., Si_3N_4 and $Si(NH)_2$, each Si atom is bonded directly to four N atoms and, in addition, H is bonded to N.

Current applications of a-$Si_xN_yH_z$ alloys involve films which are typically deposited at low T_s ($<400\,^\circ C$), so that H is unavoidably incorporated. In order to be useful, these films should be thermally stable and also should be free of Si—Si bonds.[8] It is becoming clear that silicon diimide films a-$Si(NH)_2$ have the potential to satisfy both of these requirements. The results presented here indicate that films with compositions close to that of silicon diimide, i.e., with a [N]/[Si] ratio greater than 1.9 and with low concentrations of Si—Si bonds (less than 9×10^{20} cm^{-3}), can be deposited via PECVD at $T_s=400\,^\circ C$ using $[NH_3]/[SiH_4]$ ratios equal to 40. It is important to stress that these films are not porous and are, in fact, quite stable with respect to exposure to O_2 and H_2O in the atmosphere, in contrast to some diimide-like films prepared at lower T_s.

It is clear that the high $R=[NH_3]/[SiH_4]$ ratios which are needed in the discharge in order to minimize N(Si—Si) are necessary due to the fact that SiH_4 is easier to dissociate[30] than NH_3. For lower values of R, the [N]/[Si] ratio falls below about 1.9 and there are no longer enough N atoms in the films to satisfy all of the bonds to the Si atoms, especially when it is recognized that N—H bonds are also formed. As a result, Si—Si and also Si—H bonds appear in the films. It has been observed here that the presence of Si—Si bonds in the films can actually be inferred from the presence of Si—H bonds, which can be detected directly via ir absorption. The bond concentration ratio [N(Si—Si)]/[N(Si—H)] has been found to be close to $\frac{1}{2}$ for the $R=10$ and $R=20$ films. It will be important to determine if this correlation can also be found for a-$Si_xN_yH_z$ films prepared by other workers.

The results obtained here for N(Si—Si) have been determined in two separate ways, with the results of the EMA analysis (Table IV) considered to be more reliable than those obtained from the analysis of the ir absorption and film density measurements (Table III). For the $R=40$, N-rich films, however, the results of the two analyses are in fact consistent with each other.

It has been found to be difficult, if not impossible, to deposit a-$Si_xN_yH_z$ films in which the concentration of Si—Si bonds is less than about 1%, or 9×10^{20} cm^{-3}. This low concentration cannot be accurately inferred from ir absorption and film density measurements. It has been shown, however, that such a level can be detected from careful measurements of ϵ_2, the imaginary part of the optical dielectric function. Even at this low level, the optical properties of the N-rich films are influenced significantly by the presence of the Si—Si bonds. For example, the tetrahedron model presented in the preceding paper has predicted (see Fig. 8 of Ref. 7) that E_{opt} should approach about 6.2 eV and that n should be near 1.7 for diimidelike films with $y/x>1.9$. For the $R=40$ films studied here with y/x equal to about 1.9, however, it has been found that $E_{opt}=5.2-5.4$ eV and $n=1.79-1.82$. The EMA analysis employed here has shown that this difference is due to the presence of Si—Si bonds at the level previously mentioned (9×10^{20} cm^{-3}). In addition, it has been found that the EMA analysis which has been employed is capable of establishing the existence of Si atoms bonded to either one or two other Si atoms. More work will be required in order to make this analysis more quantitative.

ACKNOWLEDGMENTS

We wish to thank D. V. Tsu of North Carolina State University for his interest in this research and for many helpful discussions. We also wish to thank R. Sabatini of Brookhaven National Laboratory (Upton, NY) for carrying out the SAM measurements on these films. This research has been supported by the U.S. Department of Energy under Grant No. DE-FG02-87ER45317.

[1]For useful reviews, see C. E. Morosanu, Thin Solid Films **65**, 171 (1980); A. C. Adams, in *Proceedings of the Symposium on Reduced Temperature Processing for VLSI*, edited by R. Reif and S. R. Srinivasan (Electrochemical Society, Pennington, NJ, 1986), Vol. 86-5.

[2]K. D. Mackenzie, A. J. Snell, I. French, P. G. Lecomber, and W. E. Spear, Appl. Phys. A **31**, 87 (1983).

[3]H. J. Stein and H. A. R. Wegener, J. Electrochem. Soc. **124**, 908 (1977).

[4]D. V. Tsu, G. Lucovsky, and M. J. Mantini, Phys. Rev. B **33**, 7069 (1986); G. Lucovsky and D. V. Tsu, J. Vac. Sci. Technol. A **5**, 2231 (1987).

[5]D. Jousse, J. Kanicki, D. T. Krick, and P. M. Lenahan, Appl. Phys. Lett. **52**, 445 (1988).

[6]R. C. Budhani, S. Prakash, H. J. Doerr, and R. F. Bunshah, J. Vac. Sci. Technol. A **5**, 1644 (1987).

[7]Z. Yin and F. W. Smith, this issue, the preceding paper, Phys. Rev. B **42**, 3658 (1990).

[8]D. Jousse and J. Kanicki, Appl. Phys. Lett. **55**, 1112 (1989).

[9]K. Mui, D. K. Basa, F. W. Smith, and R. Corderman, Phys. Rev. B **35**, 8089 (1987).

[10]D. E. Aspnes and A. A. Studna, Phys. Rev. B **27**, 985 (1983); H. R. Philipp, J. Appl. Phys. **43**, 2836 (1972).

[11]J. Tauc, R. Grigorovici, and A. Vancu, Phys. Status Solidi **15**, 627 (1966).

[12]C. J. Mogab, J. Electrochem. Soc. **120**, 932 (1973); H. R. Philipp, J. Appl. Phys. **50**, 1053 (1979).

[13]M. Maeda and H. Nakamura, J. Appl. Phys. **58**, 484 (1985).

[14]G. Lucovsky, Solid State Commun. **29**, 571 (1979).

[15]M. Cardona, Phys. Status Solidi B **118**, 463 (1983).

[16]Y. N. Volgin, G. P. Dubrovskii, and Y. I. Ukhanov, Fiz. Tverd. Tela (Leningrad) **17**, 1671 (1975) [Sov. Phys.—Solid State **17**, 1089 (1975)].

[17]T. S. Ericksson and C. G. Granqvist, J. Appl. Phys. **60**, 2081

(1986).

[18]W. A. P. Claassen, W. G. J. N. Valkenburg, M. F. C. Willemsen, and W. M. v. d. Wijgert, J. Electrochem. Soc. **132**, 893 (1985).

[19]W. A. P. Claassen, W. G. J. N. Valkenburg, F. H. P. M. Habraken, and Y. Tamminga, J. Electrochem. Soc. **130**, 2419 (1983).

[20]W. A. Lanford and M. J. Rand, J. Appl. Phys. **49**, 2473 (1978).

[21]A. D. Yadav and M. C. Yoshi, Thin Solid Films **59**, 313 (1979); A. Chayahara, M. Ueda, T. Hamasaki, and Y. Osaka, Jpn. J. Appl. Phys. Pt. 1 **24**, 19 (1985); C. Chaussat, E. Bustarret, J. C. Bruyere, and R. Groleau, Physica B+C (Amsterdam) **129B**, 215 (1985); S. Hasegawa, M. Matuura, H. Anbutu, and Y. Kurata, Philos. Mag. B **56**, 633 (1987).

[22]E. Bustarret, M. Bensouda, M. C. Habrard, J. C. Bruyere, S. Poulin, and S. C. Gujrathi, Phys. Rev. B **38**, 8171 (1988).

[23]H. R. Philipp, J. Electrochem. Soc. **120**, 295 (1973).

[24]N. Ibaraki and H. Fritzsche, Phys. Rev. B **30**, 5791 (1984); B. Dunnett, D. J. Jones, and A. D. Stewart, Philos. Mag. B **53**, 159 (1986).

[25]D. A. G. Bruggemann, Ann. Phys. (Leipzig) [Folge 5] **24**, 636 (1935).

[26]F. W. Smith, J. Appl. Phys. **55**, 764 (1984).

[27]K. Mui and F. W. Smith, Phys. Rev. B **38**, 10 623 (1988).

[28]D. E. Aspnes and J. B. Theeten, J. Appl. Phys. **50**, 4928 (1979).

[29]H. R. Philipp, J. Phys. Chem. Solids **32**, 1935 (1971).

[30]S. V. Nguyen, J. Vac. Sci. Technol. B **4**, 1159 (1986).